# O(P-3) Atoms as a Chemical Probe of Surface Ordering in Ionic Liquids

**ARTICLE** *in* THE JOURNAL OF PHYSICAL CHEMISTRY A · MARCH 2010

Impact Factor: 2.69 · DOI: 10.1021/jp912045j · Source: PubMed



**5 AUTHORS**, INCLUDING:

Carla Kidd
University of Leeds
**12** PUBLICATIONS **186** CITATIONS
SEE PROFILE

Paul A.J. Bagot
University of Oxford
**42** PUBLICATIONS **562** CITATIONS
SEE PROFILE

Matthew L Costen
Heriot-Watt University
**60** PUBLICATIONS **1,011** CITATIONS
SEE PROFILE

Kenneth G Mckendrick
Heriot-Watt University
**91** PUBLICATIONS **1,470** CITATIONS
SEE PROFILE

# $O(^3P)$ Atoms as a Chemical Probe of Surface Ordering in Ionic Liquids†

**Carla Waring, Paul A. J. Bagot, John M. Slattery,‡ Matthew L. Costen, and Kenneth G. McKendrick***

*School of Engineering and Physical Sciences, Heriot-Watt University, Edinburgh EH14 4AS, U.K.*

*Received: December 21, 2009; Revised Manuscript Received: February 18, 2010*

The reactivity of photolytically generated, gas-phase, ground-state atomic oxygen, $O(^3P)$, with the surfaces of a series of 1-alkyl-3-methylimidazolium bis(trifluoromethylsulfonyl)imide ($[NTf_2]$) ionic liquids has been investigated. The liquids differ only in the length of the linear $C_nH_{2n+1}$ alkyl side chain on the cation, with $n = 2$, 4, 5, 8, and 12. Laser-induced fluorescence was used to detect gas-phase OH $v' = 0$ radicals formed at the gas−liquid interface. The reactivity of the ionic liquids increases nonlinearly with $n$, in a way that cannot simply be explained by stoichiometry. We infer that the alkyl chains must be preferentially exposed at the interface to a degree that is dependent on chain length. A relatively sharp onset of surface segregation is apparent in the region of $n = 4$. The surface specificity of the method is confirmed through the nonthermal characteristics of both the translational and rotational distributions of the OH $v' = 0$. These reveal that the dynamics are dominated by a direct, impulsive scattering mechanism at the outer layers of the liquid. The OH $v' = 0$ yield is effectively independent of the bulk temperature of the longest-chain ionic liquid in the range 298−343 K, also consistent with a predominantly direct mechanism. These product attributes are broadly similar to those of the benchmark pure hydrocarbon liquid, squalane, but a more detailed analysis suggests that the interface may be microscopically smoother for the ionic liquids.

## Introduction

Ionic liquids (ILs) comprise a class of salts with melting points below ∼100 °C. They are composed solely of ions, giving rise to a number of unique physical and chemical properties such as negligible vapor pressure, low volatility and high thermal stability. These attributes make ILs attractive as green solvents, replacing traditional organic chemicals,[1] and in a varied range of applications spanning catalysis,[2] fuel cells,[3] electrospray thrusters,[4,5] nanoparticle formation,[6,7] antielectrostatic coatings,[8] and vapor detection.[9]

An understanding of the way ionic liquids function in many of these applications is dependent on a detailed structural knowledge of the gas−liquid interface. The relatively large cations and, in some cases, anions that give ionic liquids their desired low melting points also make a complete understanding of their interfacial structures more difficult than for simpler, high-melting-point ionic crystals. For the more complex IL systems it is no longer clear whether the gas−liquid interfacial composition resembles that of the bulk.

A widely studied class of ILs is based on 1,3-dialkylimidazolium cations. Adjusting the size of the alkyl groups on these ions offers a convenient method of tuning the properties of the liquid. $C_nH_{2n+1}$ chain lengths up to $C_{12}$ are routinely studied.[10] To probe the surface orientation of these ions, a number of experimental techniques have been employed, including direct recoil spectroscopy (DRS),[10,11] sum-frequency generation vibrational spectroscopy,[12−15] Rutherford backscattering,[16] (X-ray) photoelectron spectroscopy,[17−21] X-ray diffraction,[22] and neutron reflectivity.[23] Alongside this experimental effort, molecular dynamics simulations of 1,3-dialkylimidiazolium cations with several types of anion have been used to investigate a range of IL properties concerning both bulk and interfacial regions.[24−37]

A common observation in this literature is that the interfacial composition and order differ from those of the bulk, with the longest alkyl chain on the cation noted to project out into the vacuum,[12,14,21,33] even forming multilayer lamellar-like structures with both charges localized between alkyl-rich layers.[23] However, there is far from a universal consensus on this, with some studies suggesting that no ion segregation takes place, with the alkyl groups pointing along or even down into the liquid.[10,11] Recent work has suggested that the presence of water can play a role in determining surface properties,[15,38] as does the anion size.[20] The ability to model the surfaces correctly is dependent on a sufficiently refined treatment. For example, it has been shown that neglecting polarizability effects adversely affects the accuracy of molecular dynamics simulations.[32] This was demonstrated, for example, through calculations of the surface tension on [1,3-ethylmethylimidiazolium][$NO_3$], with results that are in much better agreement with the extrapolated experimental values when polarization effects are included.[28]

In the current study, the aspect we address is the interfacial reactivity of $[C_n$mim$][NTf_2]$ (representing 1-alkyl-3-methylimidazolium bis(trifluoromethylsulfonyl)imide) ionic liquids with gas-phase, ground-state atomic oxygen, $O(^3P)$. One of the lower members of this series, [emim] (1-ethyl-3-methylimidazolium) $[NTf_2]$, has specifically been earmarked as a candidate for thruster systems.[5] This particular reaction is therefore of relevance to space applications because $O(^3P)$ is the majority atmospheric species at the altitudes (200−700 km) of low-Earth orbit (LEO). Constituents of thrusters will be subject to reaction with $O(^3P)$ at hyperthermal collision energies because of the orbital motion of the spacecraft through the stationary atmosphere.[39]

In the experiments we report here, we use laser photolysis to generate significantly lower-energy $O(^3P)$ atoms. Relative OH

† Part of the special section "30th Free Radical Symposium".

* Corresponding author. E-mail: k.g.mckendrick@hw.ac.uk.

‡ Current address: Department of Chemistry, University of York, Heslington, York, YO10 5DD, U.K.

10.1021/jp912045j 
Published on Web 03/10/2010

product yields from a range of 1-alkyl-3-methylimidazolium [$NTf_2$] liquids are monitored by laser-induced fluorescence (LIF). This method, and an independent complementary molecular-beam approach with higher-energy O($^3$P) atoms,[40−44] have proven to be sensitive probes of surface ordering and the reaction dynamics in related studies of O($^3$P) atoms with hydrocarbon liquids.[45−50] This work forms part of an emerging field of dynamical investigations of collisions between gases and liquids that is providing growing insight into the properties of other gas−liquid[40,51−55] and related interfaces.[56−58]

We present here measurements of the relative reactivity of the series 1-alkyl-3-methylimidazolium ([$C_n$mim], spanning the range $n = 2-12$, including ethyl, *n*-butyl, *n*-pentyl, *n*-octyl, and *n*-dodecyl) [$NTf_2$] salts. All reactivities are calibrated against the "benchmark" hydrocarbon liquid, squalane ($C_{30}H_{62}$, 2,6,10,15,19,23-hexamethyltetracosane). This work is an extension of an earlier preliminary report, where we explored the relative reactivity of only the first and last members in the series, [emim][$NTf_2$] and [$C_{12}$mim][$NTf_2$].[59] We found there that [emim][$NTf_2$] had effectively negligible reactivity with our low-energy but broadly dispersed (mean 15.8 kJ mol$^{-1}$ fwhm 26 kJ mol$^{-1}$) O($^3$P) atoms. The longer-chain [$C_{12}$mim][$NTf_2$] had a much greater (more than 2 orders of magnitude) and easily detectable reactivity, although still somewhat less (∼60%) than that of liquid squalane. We concluded that stoichiometric differences between these two ionic liquids were insufficient to explain the observed gulf in reactivity. Preferential ordering of the alkyl chains at the interface, dependent on the chain length, must also play a role. The differences in reactivity between [$C_{12}$mim][$NTf_2$] and squalane suggested that this IL surface was not saturated in alkyl chains. A complementary parallel study has been carried out by Minton and co-workers[60] on identical samples of the same two ionic liquids using their alternative molecular beam source of higher energy O($^3$P) atoms (520 kJ mol$^{-1}$) coupled with angle-resolved mass-spectrometric detection. They observed both the inelastically scattered O and the reactive products OH and, at much lower intensity, $H_2O$. These molecular-beam scattering results were compared with earlier data on squalane[41,42] and were coreported with supporting, all-atom molecular dynamics simulations of the IL interfacial structures. The same qualitative sequence of relative reactivity ([emim][$NTf_2$] < [$C_{12}$mim][$NTf_2$] < squalane) was observed, but the difference between the two ionic liquids was much less marked (∼1:17) than in our photolytically based experiments (<1:250).[59] We concluded that this was a consequence of a preferential reactivity toward secondary H−C bonds in the photolytic experiments that is absent for the higher energy O($^3$P) in the molecular-beam experiments. Nevertheless, the molecular-beam experiments still yielded a reactivity ratio for [emim][$NTf_2$] and [$C_{12}$mim][$NTf_2$] that is considerably more extreme than expected on the basis of stoichiometry alone. The detailed scattering dynamics were interpreted as showing that the ionic liquids present a stiffer surface than squalane, with this effect being progressively more pronounced for [emim][$NTf_2$] than for [$C_{12}$mim][$NTf_2$]. Supported by the MD simulations, the ionic liquid surfaces were concluded to consist of both ion types, but with an overrepresentation of the longer alkyl chains at the extreme outer layers.

In the current work, we aim to understand in greater detail how the relative reactivity with O($^3$P) atoms changes with the alkyl chain length, and how this might be correlated with surface ordering. In addition to expanding the relative reactivity measurements to cover intervening chain lengths, we also extend our preliminary work[59] by presenting more details of the OH product internal distributions. We demonstrate how these are correlated with the OH translational energy for a selection of the longer-chain ionic liquids. This information can only be gained through state-selective measurements such as our spectroscopically based method. It helps to provide further insight into the reaction mechanism. The results of essentially all previous studies of reactive and inelastic scattering from hydrocarbons and some other liquids can be divided, at least empirically, into two limiting mechanisms. One component is direct, dynamically controlled impulsive scattering (IS) at the outer layers of the liquid. The other is thermal desorption (TD), in which products are accommodated at the surface and take on near-thermal translational and rotational energy distributions before being desorbed. This separation should not be taken too literally, because realistic dynamical simulations[61−65] consistently suggest that there is a continuum of interaction times with the surface and a correspondingly complex range of microscopic mechanisms. Nevertheless, the binary separation remains useful for the purposes of phenomenological characterization of experimental data and, in particular, the comparison between systems. The apparent balance between them is influenced by the surface ordering; we report here that there are experimentally distinguishable differences in this respect between the ILs and the previously most-studied pure hydrocarbon, squalane. We also present corroborating evidence from selected measurements as a function of ionic liquid temperature. From the point of view of the use of O($^3$P) (or other gas-phase projectiles) as a "chemical probe" of liquid-surface ordering, we demonstrate the important proposition that a large majority of the observed products can be attributed to direct processes at the extreme outer layers of the liquid.

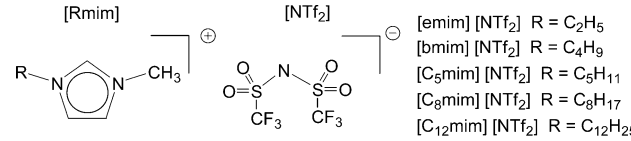


**Figure 1.** Chemical structures and nomenclature for the 1-alkyl-3-methylimidazolium-based ionic liquids.

## Experimental Section

The experimental setup has been adapted from that described previously for the investigation of the reaction dynamics of O($^3$P) and liquid hydrocarbons.[45−50] Central to the apparatus is a 5 cm diameter stainless steel wheel, housed within a vacuum chamber. The wheel is partially immersed in a copper bath filled with the liquid under investigation. Rotation of the wheel at 0.5 Hz generates a continually refreshed liquid surface. The [$C_n$mim][$NTf_2$] ionic liquids used were synthesized using modified literature procedures.[66] Halide contents were minimized by repeatedly washing the ILs with distilled water, until an $AgNO_3$ test of the separated water layer proved negative. The ILs were dried in vacuo (∼$10^{-2}$ mbar, at 70 °C for several hours). Final halide and water contents are usually well below 100 ppm and 50 ppm, respectively, using these procedures.

In practice, five ionic liquids were investigated [emim][$NTf_2$], [bmim][$NTf_2$], [$C_5$mim][$NTf_2$], [$C_8$mim][$NTf_2$], and [$C_{12}$mim][$NTf_2$] (see Figure 1 for definitions), with structures differing only in the length of the 1-alkyl chain. The liquid hydrocarbon squalane ($C_{30}H_{62}$, 2,6,10,15,19,23-hexamethyltetracosane), for which the interfacial reactivity with O($^3$P) has been extensively studied by us[45−47,49] and by the Minton group[41,42] previously, was used as a reference against which to quantify the relative reactivity of the ionic liquids. The inert perfluoropolyether (PFPE) Krytox 1506 (F-[$CF(CF_3)CF_2O$]$_{14ave}$-

$CF_2CF_3$,) was also used to check for potential artifacts due to OH that might be generated in processes other than the reaction at the liquid surface. Prior to each experiment, the ionic liquid sample was heated using a Peltier heating element to 70 ± 3 °C for ~24 h under vacuum, to ensure thorough degassing and to remove any residual water.

The O($^3$P) atoms were generated by photolyzing a carefully controlled pressure (nominally 1 mTorr) of $NO_2$ (BOC, 98.3%) at a fixed average distance of 4 mm above the liquid surface. This was achieved using the third harmonic of a Nd:YAG laser (Continuum Surelite II-10), supplying 355 nm light pulses of width 4−6 ns at 10 Hz in a 4 mm diameter beam. The laser energy was maintained at a constant value of around 70 mJ per pulse, measured at the entry to the vacuum chamber. The spatial distribution of the O($^3$P) produced in this manner is described by an anisotropy parameter, $\beta = +0.7$.[67] The photolysis laser was horizontally polarized, so roughly half of the O($^3$P) was directed toward the liquid surface. The collision energy of the O($^3$P) atoms is broadly distributed around an average value of 15.8 kJ mol$^{-1}$ (with a fwhm of 26 kJ mol$^{-1}$) in the laboratory frame, corresponding to an average speed of 1340 ms$^{-1}$.[67]

When the O($^3$P) atoms impact the liquid surface, some of them extract hydrogen atoms, generating OH $X^2\Pi$ radicals. An (unknown) fraction of these escape from the surface and are detected by LIF excited by the probe pulse, generated by a Nd:YAG-pumped dye laser. This supplied ca. 1 mJ, 4−6 ns pulses, again measured at the opposite entrance to the vacuum chamber. The probe beam (also 4 mm diameter) counterpropagated the photolysis beam, passing at the same carefully controlled centerline-distance from the surface. In the current work we have only attempted to detect vibrational ground-state OH on the $A^2\Sigma^+-X^2\Pi$ (1,0) band. The returning A−X fluorescence was collected by a liquid light guide mounted 2 cm directly above the common laser axis and directed through appropriate interference filters to a photomultiplier tube.

As explained more fully below, experiments could be split into two basic types. The first were *appearance profiles*, acquired by varying the time delay between the photolysis and probe lasers. These provide partially resolved information on the translational energy of the escaping OH species in a particular rotational (and fine-structure and Λ-doublet) state of $v' = 0$. The second were LIF *excitation spectra*, acquired by scanning the wavelength of the probe laser at a fixed photolysis-probe delay. In the current work, excitation spectra were recorded at time delays corresponding to the rising edge (5 μs), peak (9 μs), and tail (23 μs) of the appearance profiles. These spectra yield information on the product rotational (and fine-structure, etc.) state distributions. To extract nascent populations, the spectra were compared with those from a known "thermalized" distribution, as we have described in our previous work.[45−47,49] The thermal excitation spectra were recorded at a typical pressure of 100 mTorr of $N_2$ (with ~1 mTorr $NO_2$) and a photolysis-probe delay of 30 μs, corresponding to an average of approximately 30 collisions based on a typical gas-kinetic collision rate constant of $10^7$ Torr$^{-1}$ s$^{-1}$.

## Results

**Appearance Profiles.** ***Relative Reactivity Measurements.*** The relative reactivity of each of the series of $[C_n\text{mim}][NTf_2]$ liquids was measured against the well-studied reference liquid, squalane. Appearance profiles were recorded by fixing the probe laser wavelength on a specific OH A−X transition, usually the $Q_1(1)$ transition, and varying the delay time between the photolysis and probe laser. There was a background signal

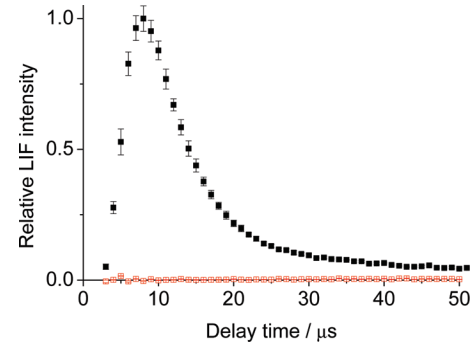


**Figure 2.** Representative appearance profiles recorded on the $Q_1(1)$ line of the OH A−X (1,0) band. Photolysis and probe-laser background signals have been subtracted, as described in the text. Liquids used were the squalane reference (black filled squares) and the inert "blank" PFPE (red open squares). Bath temperature = 298 K; $p(NO_2) \sim 1$ mTorr; surface−probe laser distance = 4 mm.

underlying each of the raw profiles, which originates from two sources. The first is caused by the photolysis laser pulse, which results in the emission of photons that are observed in both the signal gate and a gate prior to the probe-laser pulse used to establish the electronic baseline. The overall effect is an apparent negative contribution to the signal. This becomes large at very short delays, but these precede the onset of the LIF signal excited from the returning wave of OH from the surface. The second source is a small, time-independent signal, caused by probe-laser beam scatter and any probe-induced photolysis (and subsequent LIF of OH) of a minor OH-containing impurity in the $NO_2$. Therefore, background profiles were recorded by systematically blocking the photolysis and probe lasers in sequence. Both these background signals were then subtracted from the raw appearance profiles. This should yield the true OH appearance profiles resulting only from the reaction of O($^3$P) atoms at the surface.

For a given ionic liquid, repeated (typically 10) appearance profiles were recorded. We took particular care that factors such as the probe laser energy, $NO_2$ precursor pressure, and wheel−laser axis distance remained as constant as possible. Other than in specific cases indicated below, the liquid temperature was maintained at 25 °C. The wheel was removed immediately and cleaned thoroughly and the bath refilled with the squalane reference. Appearance profiles were then recorded from squalane under otherwise essentially identical conditions. Preliminary heating and degassing was found not to be necessary for squalane, as expected since it is unlikely to contain significant amounts of dissolved water. In the analysis below, we assume that the ratio of the peaks in the respective appearance profiles reflects the reactivity of each liquid relative to squalane.

An important test of the experimental procedure was to confirm that the observed signals were free from artifacts due to other potential OH-producing processes. For this purpose we used PFPE, an inert liquid containing no abstractable hydrogens, as a "blank". As in the case of the ionic liquids, the PFPE was heated to 70 °C for ~24 h before the experiments. The resulting appearance profiles and those of the squalane reference are shown in Figure 2. The profiles for squalane have the form expected from our previous work.[45−50] They contain a characteristic initial "dead time" as the O($^3$P) atoms travel to the liquid surface and the OH returns to the probe volume. The OH signal rises sharply, reaching a peak at a time delay consistent with the known distances, the average incoming O($^3$P) speed of 1340 ms$^{-1}$, and sensible recoil speeds for directly scattered OH (see

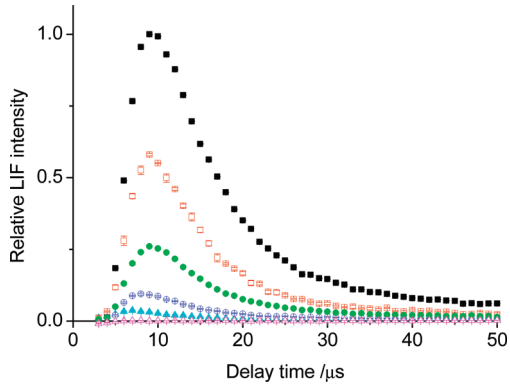


**Figure 3.** Representative appearance profiles recorded on the $Q_1(1)$ line of the OH A−X (1,0) band. Background signals resulting from the photolysis and probe lasers have been subtracted, as described in the text. Squalane (black filled squares) was used as the reference in each case. Ionic liquids were [emim][$NTf_2$] (magenta open triangles), [bmim][$NTf_2$] (cyan closed triangles), [$C_5$mim][$NTf_2$] (blue open circles), [$C_8$mim][$NTf_2$] (green filled circles), [$C_{12}$mim][$NTf_2$] (red open squares). Bath temperature = 298 K; $p(NO_2) \sim 1$ mTorr; surface−probe laser distance = 4 mm.

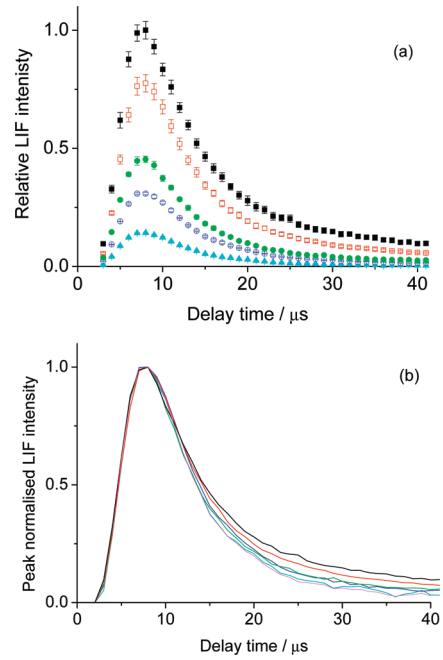


**Figure 4.** Representative appearance profiles recorded on the $Q_1(1)$ line of the OH A−X (1,0) band, from squalane. (a) Recorded at $p(NO_2)$ ~ 4 mTorr (black closed squares), ~ 3 mTorr (red open squares), ~ 1.5 mTorr (green filled circles), ~1 mTorr (blue open circles), and ~0.5 mTorr (cyan filled triangles). (b) Data represented having been peak normalized, $p(NO_2)$ ~ 4 mTorr (black line), ~ 3 mTorr (red line), ~ 1.5 mTorr (green line), ~1 mTorr (blue line), and ~0.5 mTorr (cyan line), profile at a hypothetical zero pressure (magenta line). Bath temperature = 298 K; surface−probe laser distance = 4 mm.

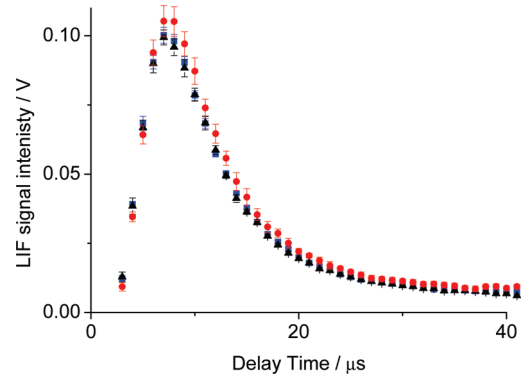


**Figure 5.** Measured appearance profiles of OH ($v' = 0$) raw LIF signals for [$C_{12}$mim][$NTf_2$] recorded at 298 K (blue squares), 323 K (black triangles) and 343 K (red circles). Profiles recorded on $Q_1(1)$ line of the OH A−X (1,0) band, shown following background subtraction as described in the text. Error bars represent the $2\sigma$ standard error in the mean of repeated measurements. $p(NO_2) \sim 1$ mTorr; surface−probe laser distance = 4 mm.

below). The appearance profiles from PFPE, however, are in stark contrast. There is no perceptible OH above the limiting signal-to-noise level, verifying that spurious OH production is indeed negligible.

This experimental procedure was repeated for each of the ionic liquids (Figure 3). As noted above, results for [emim][$NTf_2$] and [$C_{12}$mim][$NTf_2$] have been reported previously.[59] Only trace amounts of OH were detected from [emim][$NTf_2$], comparable with the overall sensitivity of the measurement. The very small, apparently negative signals in Figures 2 (PFPE) and 3 ([emim][$NTf_2$]) at early time delays result from the imperfect subtraction of the background due to the photolysis laser. The size and scatter in this artificial signal are the major sources of both statistical and systematic uncertainties in the level of any observed genuine OH signal from [emim][$NTf_2$]. We have estimated a corresponding upper limit to the reactivity of [emim][$NTf_2$] relative to squalane of 0.0025:1 (see Table 1). Appearance profiles of the intermediate chain-length ionic liquids [bmim][$NTf_2$], [$C_5$mim][$NTf_2$], and [$C_8$mim][$NTf_2$] are also included in Figure 3, and their reactivity ratios (based on at least three independent measurements per liquid) are given in Table 1. A key observation from the collected results in Figure 3 and Table 1 is that the reactivity quite clearly varies systematically, but not in a simple linear fashion, with alkyl chain length, as we discuss further below.

***Precursor-Pressure Dependence.*** As we discuss further below, an important consideration when attempting to quantify empirical IS and TD contributions is the range of delay times containing genuinely nascent OH signals. To determine the effects of secondary collisions, OH appearance profiles were measured from squalane at a variety of $NO_2$ precursor pressures. The results are shown in Figure 4a. As expected, the peak intensity (proportional to the amount of OH formed at the surface) increases approximately linearly with precursor pressure. However, the ratio of the signal at longer times to that at the peak increases as the pressure increases. We attribute this to a higher proportion of OH molecules suffering secondary collisions in the gas phase after exiting the surface, resulting in a buildup of a background of translationally thermalized OH in the observation zone. This effect is more obvious in Figure 4b, where the profiles have been peak-normalized. The differences

**TABLE 1: Summary of Repeated Independent Measurements of Relative Reactivity Ratios of the Series of [$C_n$mim][$NTf_2$] Ionic Liquids with O($^3$P), Each Compared to Squalane as the Reference[a]**

| cation | [emim][$NTf_2$] | [bmim][$NTf_2$] | [$C_5$mim][$NTf_2$] | [$C_8$mim][$NTf_2$] | [$C_{12}$mim][$NTf_2$] |
|---|---|---|---|---|---|
| IL:Sq | 0.0025[b]:1 | 0.038 ± 0.004:1 | 0.09 ± 0.02:1 | 0.27 ± 0.01:1 | 0.62 ± 0.06:1 |

[a] Error quoted is the $2\sigma$ standard error in the mean. [b] Estimated upper limit on reactivity.

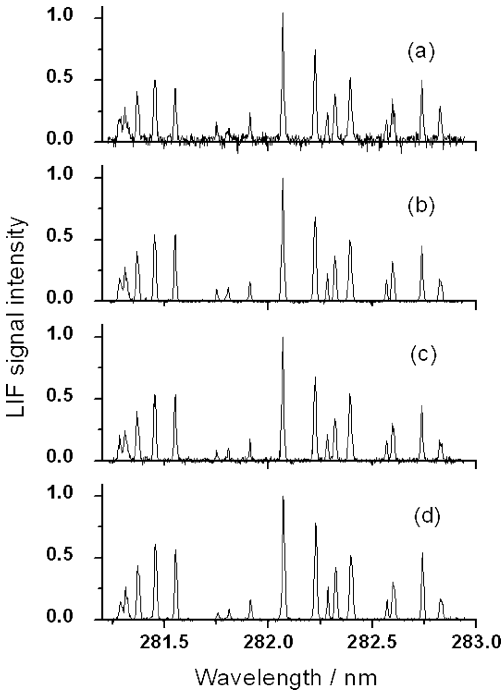


**Figure 6.** Representative OH A−X (1,0) LIF excitation spectra from $[C_{12}mim][NTf_2]$. Nascent spectra recorded at photolysis-probe laser delays of (a) 5 $\mu$s, (b) 9 $\mu$s, and (c) 23 $\mu$s. (d) Thermal spectrum at a photolysis-probe laser delay of 30 $\mu$s, $p(NO_2) \sim 1$ mTorr and $p(N_2) \sim 0.1$ Torr. Probe laser−liquid surface distance = 4 mm.

clearly become progressively more significant at later times for the higher pressures, consistent with a collisional process. It is possible to generate a hypothetical "zero-pressure" profile, also included in Figure 4b, by linear extrapolation of the normalized signals at each time delay. Although the rising edges are essentially identical, it is clear that on the trailing edge the difference between the hypothetical zero-pressure profile and that at 1 mTorr (the pressure used for the main body of our experiments) is no longer negligible. We therefore take due note of this when comparing Monte Carlo simulations of the profiles to the experimental data in the discussion that follows below.

***Liquid-Temperature Dependence.*** OH appearance profiles from the longest-chain ionic liquid, $[C_{12}mim][NTf_2]$, were also recorded at three different bulk liquid temperatures of 298, 323, and 343 K, as shown in Figure 5. Great care was taken to ensure consistency in other experimental parameters such as precursor pressure and probe laser energy, etc. It is clear that there is very little variation in either the peak height or shape of the profile, with any such differences lying within the statistical uncertainties.

**LIF Excitation Spectra.** We have recorded OH LIF excitation spectra from the $[C_{12}mim][NTf_2]$ ionic liquid, at photolysis-probe delays of 5, 9, and 23 $\mu$s, corresponding to the rising edge, peak, and tail of the appearance profile, respectively. A representative set of spectra is shown in Figure 6. As in our previous work, the spectra were analyzed by constructing Boltzmann plots from which nominal temperatures could be extracted. Rotational temperatures were determined for three of the six OH A−X main branches, $Q_1$, $R_1$, and $R_2$. These were then averaged together with a weighting according to their relative populations in a 300 K sample, i.e., 70% $F_1$ and 30% $F_2$. This process was repeated seven times altogether, from which the overall average rotational temperature for each time delay was determined as listed in Table 2. There is a clear correlation with delay time. The highest temperature (372 ± 16 K) was found at the shortest delay, but even those at longer delays remain at least slightly superthermal.

**TABLE 2: Rotational Temperatures of Nascent OH ($v' = 0$) Formed by Reaction of ($O^3P$) Atoms with $[C_{12}mim][NTf_2]$, Measured at Different Photolysis-Probe Delays[a]**

| | rising edge 5 $\mu$s | peak 9 $\mu$s | tail 23 $\mu$s |
|---|---|---|---|
| rotational temperature/K | 372 ± 16 | 340 ± 5 | 333 ± 4 |

[a] Error quoted is the 1$\sigma$ standard error in the mean.

## Discussion

Our key observation is that photolytically generated $O(^3P)$ atoms show a strong differential reactivity with the series of 1-alkyl-3-methylimidazolium based ionic liquids. We had already determined previously[59] that the reactivity differed very markedly between the first ($n = 2$) and last ($n = 12$) members of the series, consistent with the complementary results of the Minton group experiments[60] on identical samples. We have established here for the first time the form of the variation at intervening chain lengths. We consider in more detail below what the implications are for the degree of ordering at the surface as a function of chain length. First, though, we seek to demonstrate the validity of our basic premise on which this interpretation will be based, i.e., that our method is indeed surface-specific and that the observed OH is generated through reaction only at the outermost regions of the liquid.

There is actually a perfectly valid a priori argument that the fact that we detect OH radicals at all implies that they cannot have survived very many secondary encounters at the surface, simply because the barriers to abstraction of a second H atom are much lower (typically 3−10 kJ $mol^{-1}$)[68] than for the initial abstraction by $O(^3P)$. Less circumstantially, the observed appearance profiles and LIF excitation spectra provide direct evidence that the majority of the observed OH must be produced through processes that correspond more closely to the direct impulsive IS limit than to thermal desorption.

The appearance profiles for the longer-chain liquids $[C_8mim][NTf_2]$ and $[C_{12}mim][NTf_2]$, for which the signal-to-noise is sufficient to allow a sensible comparison, are replotted in peak-normalized form in Figure 7 alongside that for squalane. The overall shapes of all three profiles are relatively similar. It has already been established in previous work[69,70] that the profile for squalane is dominated by the IS contribution, so this must qualitatively also be true for the ionic liquids. There are, however, some subtle differences between the liquids, particu-

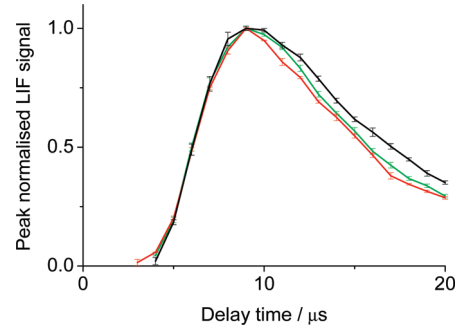


**Figure 7.** Representative peak-normalized appearance profiles recorded on $Q_1(1)$ line of the OH A−X (1,0) band, shown from squalane (black), $[C_8mim][NTf_2]$ (green), and $[C_{12}mim][NTf_2]$ (red). Background signals resulting from the photolysis and probe lasers have been subtracted, as described in the text. Bath temperature = 298 K; $p(NO_2) \sim 1$ mTorr; surface−probe laser distance = 4 mm.

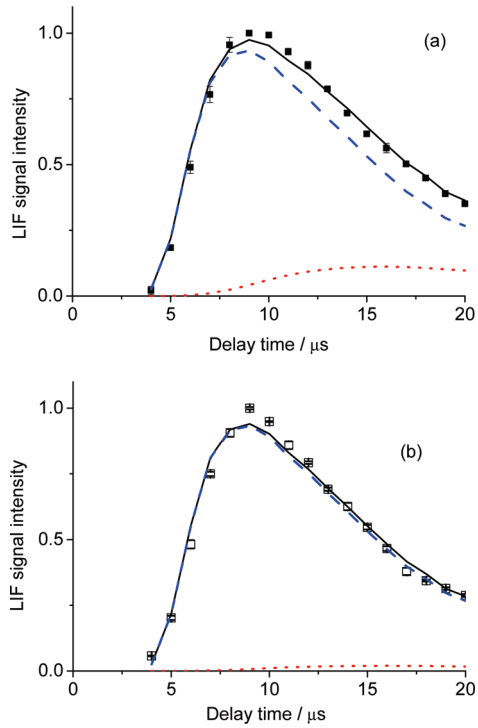


**Figure 8.** Representative appearance profiles of OH ($v' = 0$) peak-normalized LIF signals for (a) squalane (black filled squares) and (b) [$C_{12}$mim][$NTf_2$] (black open squares). Also included are Monte Carlo simulations of a direct, impulsively scattered (IS) component (blue dashed line) and a thermal (TD) component (red dotted line). The black solid line in each case represents a linear least-squares fit of weighted components to the experimental data. Bath temperature = 298 K; $p(NO_2) \sim 1$ mTorr; surface−probe laser distance = 4 mm.

larly between the two ILs and squalane at longer delays. It appears that the ionic liquids produce a smaller proportion of slower OH than squalane does.

To pursue this more quantitatively, we have carried out further Monte Carlo simulations of a similar type to those we have described previously.[46,69] The analysis assumes that the appearance profile consists of weighted contributions from limiting IS and TD mechanisms. The angular and translational energy distributions from the IS mechanism are parametrized according to the previous molecular beam scattering results for the OH from O($^3$P) + squalane by Minton and co-workers.[41,42] Those for the TD channel are generated analytically for a Maxwell−Boltzmann distribution of velocities at the bulk liquid temperature distributed in a cos$\theta$ distribution about the surface normal. Monte Carlo sampling is used to average correctly over the other experimental variables, including the distribution of O($^3$P) velocities produced by $NO_2$ photolysis and the various geometric factors related to the trajectories of O($^3$P) and OH.

Linear least-squares fits of the IS and TD components to the experimental profiles from [$C_{12}$mim][$NTf_2$] and squalane are shown in Figure 8. The fit allows for the effects of the differences in detection sensitivity due to the distinct predicted angular distributions of IS and TD components and the usual flux-density bias that favors the detection of slower-moving molecules. In carrying out the fits, we have taken note of the restriction described above, established on the basis of Figure 4, that only the first ~20 $\mu$s of the profile should be considered sufficiently free of the effects of secondary gas-phase collisions. More significantly, we have also included the thermal motion of the $NO_2$ precursor[71] that was neglected previously. This broadens the incoming velocity distribution, which is reflected

**TABLE 3: Impulsively Scattered (IS) to Thermal (TD) Ratios Obtained from Linear Least-Squares Fits of Monte Carlo Simulated Components to the Experimental Appearance Profiles[a]**

| liquid | squalane | [$C_{12}$mim][$NTf_2$] |
|---|---|---|
| IS:TD | 89:11 | 98:2 |

[a] The fit takes appropriate account of the differences in detection sensitivity due to the distinct angular distributions of IS and TD components and the flux-density bias in favor of slower-moving molecules. Purely statistical uncertainties are of the order of a few percent but are likely to be outweighed by systematic errors arising from assumptions in the modeling. As discussed in the text, the results for squalane differ from those reported previously[70] primarily due to the inclusion of thermal blurring from $NO_2$ precursor motion.

primarily in a broader IS scattered distribution. Consequently, we obtain an improved overall fit containing a somewhat smaller TD component for squalane than previously,[46,47,69,70] but the best-fit does still require a minority TD contribution to be included. We have confirmed that refitting the previous squalane data[70] produces revised IS:TD ratios essentially identical to those for squalane we present here. In contrast, the fitted TD component for [$C_{12}$mim][$NTf_2$] is almost negligible, as summarized in Table 3. We note that this is also true of the refitted data from a self-assembled monolayer (SAM) surface,[70] where previously we had deduced a TD component that was smaller than that from squalane but non-negligible.

The relatively short flight paths and substantial geometric and velocity averaging mean that our experimental velocity resolution is not particularly high. This is compounded by various assumptions subject to systematic error required in the simulations. We have already noted the significant effect on the fitted ratios of a more refined treatment of the O($^3$P) velocity distribution. Consequently, although their purely statistical uncertainties are quite small (of order a few percent in the IS fraction), these quantitative ratios should not be regarded as rigorous quite apart from the fundamental issue of whether it is valid to decompose the observed products into two limiting mechanisms. We reiterate that realistic dynamical simulations on related systems[61−65] have demonstrated that products with apparently thermal velocities do not necessarily arise from long-lived trajectories that become thermally accommodated with the surface. In reality, there is typically an extended distribution of the number of interactions with the surface and a corresponding array of distinct microscopic mechanisms. Regardless of this qualification, from the point of view of the current work the main conclusion is clear: the majority of the OH observed from the ionic liquids (and from squalane) is simply moving far too fast to have been subject to efficient secondary exchange of translational energy with the surface. It must therefore be produced in a relatively direct, ballistic process at the outer layers of the liquid. Beyond that robust primary conclusion, the modest differences between squalane and the ionic liquids are nevertheless significant and reproducible. They suggest that the [$C_{12}$mim][$NTf_2$] surface favors even more strongly a direct mechanism. This would be consistent with the ionic liquid surface being microscopically smoother than that of squalane, making the OH less likely to suffer secondary, dissipative encounters before escaping into the gas phase. This is plausible because previous MD simulations of the squalane surface[64,72] do indeed predict considerable roughness on the molecular scale as a consequence of its branched-chain structure. Similar qualitative differences in the smoothness of SAM and squalane surfaces were deduced previously.[70] As noted above, these are confirmed in the refitted SAM profiles that are best-fit with a

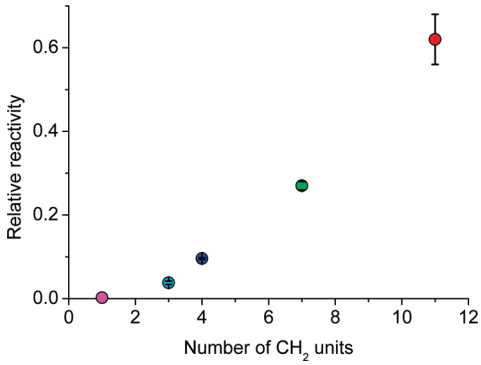


**Figure 9.** Relative reactivity (normalized to squalane) toward $O(^3P)$ atoms as a function of the number of $CH_2$ units in the 1-alkyl chain of the series of 1-alkyl-3-methylimidazolium based ionic liquids. (Fill colors match the symbols in Figure 3.) Error bars (which are smaller than the symbols for liquids other than $[C_{12}mim][NTf_2]$) show the $2\sigma$ standard error in the mean of the relative reactivity measurements for each liquid. The result for $[emim][NTf_2]$ is an upper limit, as in Table 1 and explained in the text.

near negligible TD contribution comparable to that for $[C_{12}mim][NTf_2]$.

Further evidence for a subtly different aspect of the directness of the reaction mechanism comes from the lack of a significant temperature-dependence of the OH yield from $[C_{12}mim][NTf_2]$ in Figure 5. If the incoming $O(^3P)$ atoms were translationally accommodated but then went on to react in a thermally activated mechanism, then a substantial Arrhenius-like temperature dependence would be expected. A similar lack of dependence was observed previously for squalane.[49] The implication is that for both liquids the $O(^3P)$ must react on the first, or at least a very early, encounter promoted by its incoming superthermal energy.

The final corroborating evidence for a direct mechanism is the observed OH rotational temperatures. It is clear from Figure 6 and Table 2 that at all points in the appearance profile the rotational temperature of the OH escaping from $[C_{12}mim][NTf_2]$ is significantly above the bulk liquid temperature of 298 K. The rotational temperature of $372 \pm 16$ K at the rising edge of the profile is compatible with those observed for the related (direct abstraction) reactions of $O(^3P)$ with hydrocarbons in the gas phase,[73] suggesting once again a direct mechanism. There is, though, some variation with appearance time. The slower OH appears to be rotationally somewhat cooler. This could be evidence for some secondary encounters leading to rotational relaxation of the slower OH, of which the rotational temperature is perhaps a more sensitive diagnostic than the translational energy distribution. A similar phenomenon was interpreted in this way for squalane.[47] However, we should note that there are other potential explanations, including a possible correlation between $O(^3P)$ translational energy and OH rotational excitation. In any case, the broad picture is clear that the overall elevated rotational temperatures at all points in the appearance profile are not consistent with a dominant thermal desorption mechanism.

We return now to our main observation of substantially different OH yields from the series of ionic liquids, confident that these reflect in some way the composition of the extreme outer layers because the mechanistic evidence points strongly to a dominant direct process. The differences in OH yield cannot simply be the result of molecular stoichiometry. We emphasize this point in Figure 9, where the peak OH yields from Figure 3 are plotted as a function of the number of $CH_2$ units in the 1-alkyl chain. The reason for choosing this construction is that, as mentioned in the Introduction, for $O(^3P)$ atoms with collision energies distributed around an average of 15.8 kJ mol$^{-1}$ with a fwhm of 26 kJ mol$^{-1}$, we believe there will be a strong bias toward reaction with secondary H−C units. This results directly from the considerably different barriers to abstraction (established from gas-phase measurements[73]) of typically 34 and 22 kJ mol$^{-1}$, respectively, for primary and secondary H−C bonds. Consistent values have also been predicted theoretically.[74] Therefore, if the observed reactivity of the ionic liquids had simply reflected the number of secondary H atoms, then Figure 9 would have been a straight line through the origin. It most clearly is not. The actual variation is much more complex, with effectively no perceptible reactivity for $[emim][NTf_2]$ (i.e., a single $CH_2$ unit) but then a sharp increase beyond $[bmim][NTf_2]$. The implication is that the alkyl chains become progressively more exposed at the liquid surface as the chain length increases.

In the context of the extensive current literature on the interfacial structure of $[C_nmim]$ ionic liquids, our main finding of increasing segregation at the interfaces for longer alkyl chains is consistent with the majority view, provided through a range of experimental[12,14−19,23] and theoretical studies.[26,28,29,33,35,37] Perhaps the greatest remaining discrepancies in surface structures are in those inferred from direct recoil spectroscopy measurements.[10,11] There is also independent evidence for the existence of a critical alkyl chain length of $\geq 4$ carbon atoms beyond which chain segregation at the interface is more pronounced[19,21] and can also be accompanied by aggregation of chains in the bulk.[22,25,37] In the directly relevant molecular dynamics simulations of the shortest ($[emim][NTf_2]$) and longest ($[C_{12}mim][NTf_2]$) chain systems accompanying the complementary Minton experiments,[60] these phenomena were indeed predicted. For $[emim][NTf_2]$ there is little preference for the ethyl groups to occupy the surface. In contrast, for $[C_{12}mim][NTf_2]$, there is a pronounced selectivity for alkyl groups to be present at the interface. The final six carbons of the alkyl chain are predicted to project, on average, above the surrounding anion density. These segments tend to fold over and lie approximately parallel, on average, to the plane of the surface. This is consistent with the conclusion that their secondary H atoms are efficiently exposed to attack. Some aggregation of chains at the surface is predicted, and indeed also in bulk regions.

While it is clear that the longer alkyl chains segregate at the interface, a secondary issue is what fraction of the surface is covered by them. The detailed inelastic and reactive scattering dynamics observed in the Minton work[60] imply that the surface of $[C_{12}mim][NTf_2]$ is not saturated with alkyl chains. This conclusion is supported by the accompanying MD simulations. We can explore this aspect further by comparison of the results here for the ionic liquids with our own earlier studies of $O(^3P)$ reacting with related surfaces. For linear thioalkyl self-assembled monolayers (SAMs) on gold,[70] we saw no escalation in reactivity when the hydrocarbon backbone length was increased from 6 to 18. These SAMs are known to be dense, well-ordered layers with alkyl chains inclined at an acute angle (around 30°) to the surface normal. They therefore present a completely saturated surface to an incoming $O(^3P)$ atom. The lack of any increase in reactivity beyond an alkyl chain length of 6 suggests the $O(^3P)$ atoms are unable to penetrate beyond this point, and the observed OH production must be confined to a shorter, terminal segment of the chain. This differs markedly from the results for the ionic liquids in the present work. It is apparent from, e.g., Figure 9 that the reactivity is still increasing strongly at $n = 6$ and quite probably beyond $n = 12$. This therefore strongly

supports the conclusion that the $[C_{12}mim][NTf_2]$ surface does not resemble a SAM-like monolayer of alkyl chains.

Even if there is now comparatively broad consensus across the many ionic liquid studies on some basic aspects of the surface composition, there remain a number of more detailed features that are far from securely established. For example, little is known experimentally on the angle the projecting alkyl chains make with the surface, for which there are some existing predictions from MD simulations.[29] Further uncertainties surround the existence of "lamellar-like" multilayers,[23,29,33] of oscillations in the density of the liquid with depth,[28,32,33,35] and on the orientation of the cation at the surface[75] which may be influenced by impurities[21] as well as the length of the alkyl chains.[12] Additionally, the extent of alkyl chain segregation has recently been shown to be dependent on the nature of the anion.[20] Small species such as $Cl^-$ yield a denser, more ordered alkyl chain structure than larger ones such as the $[NTf_2]$ anion used here. We suggest that gas-surface scattering, such as in the current work and in the complementary experiments of the Minton group,[60] represents a promising new approach to gaining further insight into some of these outstanding questions.

## Conclusions

We have shown that photolytically generated, superthermal gas-phase $O(^3P)$ atoms are a sensitive probe of surface ordering in [1-alkyl-3-methylimidazolium][$NTf_2$] ionic liquids. The gas-phase OH yields are a strong function of the 1-alkyl chain length of the $[C_nmim]$ cation. We interpret the yields as clear evidence for preferential, nonstoichiometric occupation of the surface by longer alkyl chains. There appears to be a threshold in the region of $\geq 4$ carbon atoms beyond which surface segregation increases. This observation is in agreement with results for related ionic liquids from a range of other experimental and theoretical methods. By comparison with the benchmark pure hydrocarbon liquid, squalane, we can also say that the surfaces of the ionic liquids are not saturated with alkyl chains, at least up to the longest length ($C_{12}$) studied.

We have established securely the surface specificity of this method by demonstrating that the reaction mechanism is predominantly direct, impulsive scattering at the outer layers of the liquid. The evidence for this includes the nonthermal nature of the OH translational and rotational energy distributions and the absence of any significant bulk-liquid-temperature dependence of the OH yield.

These product attributes are broadly similar to those of the benchmark pure hydrocarbon liquid, squalane, but there are some differences in detail. There is a lower proportion of slower OH for $[C_{12}mim][NTf_2]$ than for squalane, consistent with the interface being microscopically smoother for the ionic liquids.

Our results are consistent with those of complementary molecular beam scattering experiments by Minton and coworkers[60] on the shortest ([emim][$NTf_2$]) and longest ($[C_{12}mim][NTf_2]$) chain systems, with due recognition of the consequences of the significantly different collision energy regimes, and are supported by their accompanying molecular dynamics simulations. We propose that such methods have the potential to provide new surface-compositional information on a wide range of ionic liquids.

**Acknowledgment.** M.L.C. is supported by an RCUK Academic Fellowship. We acknowledge the financial support of the Air Force Office of Scientific Research, Air Force Material Command, USAF, under grant number FA8655-08-1-3079.

## References and Notes

(1) Holbrey, J. D.; Seddon, K. R. *Clean Prod. Process.* **1999**, *1*, 223.
(2) Pârvulescu, V. I.; Hardacre, C. *Chem. Rev.* **2007**, *107*, 2615.
(3) Cho, E.; Park, J. S.; Sekhon, S. S.; Park, G. G.; Yang, T. H.; Lee, W. Y.; Kim, C. S.; Park, S. B. *J. Electrochem. Soc.* **2009**, *156*, B197.
(4) Romero-Sanz, I.; Bocanegra, R.; Fernandez de la Mora, J.; Gamero-Castaño, M. *J. Appl. Phys.* **2003**, *94*, 3599.
(5) Chiu, Y.-H.; Gaeta, G.; Levandier, D. J.; Dressler, R. A.; Boatz, J. A. *Int. J. Mass Spectrom.* **2007**, *265*, 146.
(6) Dupont, J.; Fonseca, G. S.; Umpierre, A. P.; Fichtner, P. F. P.; Teixeira, S. R. *J. Am. Chem. Soc.* **2002**, *124*, 4228.
(7) Scheeren, C. W.; Machado, G.; Teixeira, S. R.; Morais, J.; Domingos, J. B.; Dupont, J. *J. Phys. Chem. B* **2006**, *110*, 13011.
(8) Pernak, J.; Czepukowicz, A.; Poźniak, R. *Ind. Eng. Chem. Res.* **2001**, *40*, 2379.
(9) Liang, C.; Yuan, C.-Y.; Warmack, R. J.; Barnes, C. E.; Dai, S. *Anal. Chem.* **2002**, *74*, 2172.
(10) Law, G.; Watson, P. R.; Carmichael, A. J.; Seddon, K. R. *Phys. Chem. Chem. Phys.* **2001**, *3*, 2879.
(11) Gannon, T. J.; Law, G.; Watson, P. R.; Carmichael, A. J.; Seddon, K. R. *Langmuir* **1999**, *15*, 8429.
(12) Santos, C. S.; Baldelli, S. *J. Phys. Chem. B* **2007**, *111*, 4715.
(13) Iimori, T.; Iwahashi, T.; Kanai, K.; Seki, K.; Sung, J.; Kim, D.; Hamaguchi, H.; Ouchi, Y. *J. Phys. Chem. B* **2007**, *111*, 4860.
(14) Iimori, T.; Iwahashi, T.; Ishii, H.; Seki, K.; Ouchi, Y.; Ozawa, R.; Hamaguchi, H.; Kim, D. *Chem. Phys. Lett.* **2004**, *389*, 321.
(15) Sung, J.; Jeon, Y.; Kim, D.; Iwahashi, T.; Iimori, T.; Seki, K.; Ouchi, Y. *Chem. Phys. Lett.* **2005**, *406*, 495.
(16) Ohno, A.; Hashimoto, H.; Nakajima, K.; Suzuki, M.; Kimura, K. *J. Chem. Phys.* **2009**, *130*, 204705.
(17) Smith, E. F.; Villar Garcia, I. J.; Briggs, D.; Licence, P. *Chem. Commun.* **2005**, *45*, 5633.
(18) Krischok, S.; Eremtchenko, M.; Himmerlich, M.; Lorenz, P.; Uhlig, J.; Neumann, A.; Öttking, R.; Beenken, W. J. D.; Höfft, O.; Bahr, S.; Kempter, V.; Schaefer, J. A. *J. Phys. Chem. B* **2007**, *111*, 4801.
(19) Lovelock, K. R. J.; Kolbeck, C.; Cremer, T.; Paape, N.; Schulz, P. S.; Wasserscheid, P.; Maier, F.; Steinrück, H.-P. *J. Phys. Chem. B* **2009**, *113*, 2854.
(20) Kolbeck, C.; Cremer, T.; Lovelock, K. R. J.; Paape, N.; Schulz, P. S.; Wasserscheid, P.; Maier, F.; Steinruck, H. P. *J. Phys. Chem. B* **2009**, *113*, 8682.
(21) Lockett, V.; Sedev, R.; Bassell, C.; Ralston, J. *Phys. Chem. Chem. Phys.* **2008**, *10*, 1330.
(22) Triolo, A.; Russina, O.; Bleif, H.-J.; Di Cola, E. *J. Phys. Chem. B* **2007**, *111*, 4641.
(23) Bowers, J.; Vergara-Gutierrez, M. C. *Langmuir* **2004**, *20*, 309.
(24) Morrow, T. I.; Maginn, E. J. *J. Phys. Chem. B* **2002**, *106*, 12807.
(25) Wang, Y.; Voth, G. A. *J. Phys. Chem. B* **2006**, *110*, 18601.
(26) Wang, Y.; Jiang, W.; Yan, T.; Voth, G. A. *Acc. Chem. Res.* **2007**, *40*, 1193.
(27) Yan, T.; Burnham, C. J.; Del Pópolo, M. G.; Voth, G. A. *J. Phys. Chem. B* **2004**, *108*, 11877.
(28) Yan, T.; Li, S.; Jiang, W.; Gao, X.; Xiang, B.; Voth, G. A. *J. Phys. Chem. B* **2006**, *110*, 1800.
(29) Jiang, W.; Wang, Y.; Tianying, Y.; Voth, G. A. *J. Phys. Chem. C* **2008**, *112*, 1132.
(30) Picálek, J.; Kolafa, J. *J. Mol. Liq.* **2007**, *134*, 29.
(31) Ghatee, M. H.; Ansari, Y. *J. Chem. Phys.* **2007**, *126*, 154502.
(32) Sloutskin, E.; Lynden-Bell, R. M.; Balasubramanian, S.; Deutsch, M. *J. Chem. Phys.* **2006**, *125*, 174715.
(33) Bhargava, B. L.; Balasubramanian, S. *J. Am. Chem. Soc.* **2006**, *128*, 10073.
(34) Urahata, S. M.; Ribeiro, M. C. *J. Chem. Phys.* **2004**, *120*, 1855.
(35) Lynden-Bell, R. M. *Mol. Phys.* **2003**, *101*, 2625.
(36) Lynden-Bell, R. M.; Kohanoff, J.; Del Popolo, M. G. *Faraday Discuss.* **2005**, *129*, 57.
(37) Canongia Lopes, J. N.; Pádua, A. A. H. *J. Phys. Chem. B* **2006**, *110*, 3330.
(38) Gottfried, J. M.; Maier, F.; Rossa, J.; Gerhard, D.; Schulz, P. S.; Wasserscheid, P.; Steinruck, H. P. *Z. Phys. Chem.* **2006**, *220*, 1439.
(39) Leger, L. J.; Visentine, J. T. *J. Spacecr. Rockets* **1986**, *23*, 505.
(40) Garton, D. J.; Minton, T. K.; Alagia, M.; Balucani, N.; Casavecchia, P.; Volpi, G. G. *Faraday Discuss.* **1997**, *108*, 387.
(41) Garton, D. J.; Minton, T. K.; Alagia, M.; Balucani, N.; Casavecchia, P.; Volpi, G. G. *J. Chem. Phys.* **2000**, *112*, 5975.
(42) Garton, D. J.; Minton, T. K.; Alagia, M.; Balucani, N.; Casavecchia, P.; Volpi, G. G. *J. Chem. Phys.* **2001**, *114*, 5958.
(43) Zhang, J.; Garton, D. J.; Minton, T. K. *J. Chem. Phys.* **2002**, *117*, 6239.
(44) Zhang, J.; Upadhyaya, H. P.; Brunsvold, A. L.; Minton, T. K. *J. Phys. Chem. B* **2006**, *110*, 12500.

(45) Kelso, H.; Köhler, S. P. K.; Henderson, D. A.; McKendrick, K. G. *J. Chem. Phys.* **2003**, *119*, 9985.
(46) Köhler, S. P. K.; Allan, M.; Kelso, H.; Henderson, D. A.; McKendrick, K. G. *J. Chem. Phys.* **2005**, *122*, 024712.
(47) Köhler, S. P. K.; Allan, M.; Costen, M. L.; McKendrick, K. G. *J. Phys. Chem. B* **2006**, *110*, 2771.
(48) Allan, M.; Bagot, P. A. J.; Köhler, S. P. K.; Costen, M. L.; McKendrick, K. G. *Phys. Scr.* **2007**, *76*, C42.
(49) Allan, M.; Bagot, P. A. J.; Costen, M. L.; McKendrick, K. G. *J. Phys. Chem. C* **2007**, *111*, 14833.
(50) Allan, M.; Bagot, P. A. J.; Westacott, R. E.; Costen, M. L.; McKendrick, K. G. *J. Phys. Chem. C* **2008**, *112*, 1524.
(51) Saecker, M. E.; Govoni, S. T.; Kowalski, D. V.; King, M. E.; Nathanson, G. M. *Science* **1991**, *252*, 1421.
(52) Nathanson, G. M. *Annu. Rev. Phys. Chem.* **2004**, *55*, 231.
(53) Minton, T. K.; Giapis, K. P.; Moore, T. *J. Phys. Chem. A* **1997**, *101*, 6549.
(54) Perkins, B. G.; Häber, T.; Nesbitt, D. J. *J. Phys. Chem. B* **2005**, *109*, 16396.
(55) Zolot, A. M.; Harper, W. W.; Perkins, B. G.; Dagdigian, P. J.; Nesbitt, D. J. *J. Chem. Phys.* **2006**, *125*, 021101.
(56) Isa, N.; Gibson, K. D.; Yan, T.; Hase, W.; Sibener, S. J. *J. Chem. Phys.* **2004**, *120*, 2417.
(57) Shuler, S. F.; Davis, G. M.; Morris, J. R. *J. Chem. Phys.* **2002**, *116*, 9147.
(58) Alexander, W. A.; Morris, J. R.; Troya, D. *J. Chem. Phys.* **2009**, *130*, 084702.
(59) Waring, C.; Bagot, P. A. J.; Slattery, J. M.; Costen, M. L.; McKendrick, K. G. *J. Phys. Chem. Lett.* **2010**, *1*, 429.
(60) Wu, B.; Zhang, J.; Minton, T. K.; McKendrick, K. G.; Slattery, J. M.; Yockel, S.; Schatz, G. C. *J. Phys. Chem. C* **2010**, *114*, 4015.
(61) Li, G.; Bosio, S. B. M.; Hase, W. L. *J. Mol. Struct.* **2000**, *556*, 43.
(62) Troya, D.; Schatz, G. C. *J. Chem. Phys.* **2004**, *120*, 7696.
(63) Tasić, U. S.; Yan, T.; Hase, W. L. *J. Phys. Chem. B* **2006**, *110*, 11863.
(64) Kim, D.; Schatz, G. C. *J. Phys. Chem. A* **2007**, *111*, 5019.
(65) Peng, Y.; Liu, L.; Cao, Z.; Li, S.; Mazyar, O. A.; Hase, W. L.; Yan, T. *J. Phys. Chem. C* **2008**, *112*, 20340.
(66) Bonhôte, P.; Dias, A.-P.; Papageorgiou, N.; Kalyanasundaram, K.; Grätzel, M. *Inorg. Chem.* **1996**, *35*, 1168.
(67) Baker, R. P.; Costen, M. L.; Hancock, G.; Ritchie, G. A. D.; Summerfield, D. *Phys. Chem. Chem. Phys.* **2000**, *2*, 661.
(68) Wilson, E. W. J.; Hamilton, W. A.; Kennington, H. R.; Evans, B. I.; Scott, N. W.; DeMore, W. B. J. *J. Phys. Chem. A* **2006**, *110*, 3593.
(69) Bagot, P. A. J.; Waring, C.; Costen, M. L.; McKendrick, K. G. *J. Phys. Chem. C* **2008**, *112*, 10868.
(70) Waring, C.; Bagot, P. A. J.; Räisänen, M. T.; Costen, M. L.; McKendrick, K. G. *J. Phys. Chem. A* **2009**, *113*, 4320.
(71) van der Zande, W. J.; Zhang, R.; Zare, R. N.; McKendrick, K. G.; Valentini, J. J. *J. Phys. Chem.* **1991**, *95*, 8205.
(72) Köhler, S. P. K.; Reed, S. K.; Westacott, R. E.; McKendrick, K. G. *J. Phys. Chem. C* **2006**, *110*, 11717.
(73) Ausfelder, F.; McKendrick, K. G. *Prog. React. Kinet. Mech.* **2000**, *25*, 299.
(74) Troya, D. *J. Phys. Chem. A* **2007**, *111*, 10745.
(75) Aliaga, C.; Santos, C. S.; Baldelli, S. *Phys. Chem. Chem. Phys.* **2007**, *9*, 3683.

JP912045J